Valence band offset, strain and shape effects on confined states in self-assembled InAs/InP and InAs/GaAs quantum dots

2013 J. Phys.: Condens. Matter 25 465301

(http://iopscience.iop.org/0953-8984/25/46/465301)

IOP PUBLISHING JOURNAL OF PHYSICS: CONDENSED MATTER
J. Phys.: Condens. Matter **25** (2013) 465301 (16pp) doi:10.1088/0953-8984/25/46/465301

Valence band offset, strain and shape effects on confined states in self-assembled InAs/InP and InAs/GaAs quantum dots

M Zieliński

Institute of Physics, Faculty of Physics, Astronomy and Informatics, Nicolaus Copernicus University, Grudziadzka 5, 87-100 Torun, Poland

E-mail: mzielin@fizyka.umk.pl

Received 11 April 2013, in final form 29 August 2013
Published 15 October 2013
Online at stacks.iop.org/JPhysCM/25/465301

Abstract
I present a systematic study of self-assembled InAs/InP and InAs/GaAs quantum dot single-particle and many-body properties as a function of the quantum dot–surrounding matrix valence band offset. I use an atomistic, empirical tight-binding approach and perform numerically demanding calculations for half-million-atom nanosystems. I demonstrate that the overall confinement in quantum dots is a non-trivial interplay of two key factors: strain effects and the valence band offset. I show that strain effects determine both the peculiar structure of confined hole states of lens type InAs/GaAs quantum dots and the characteristic 'shell-like' structure of confined hole states in the commonly considered 'low-strain' lens type InAs/InP quantum dot. I also demonstrate that strain leads to single-band-like behavior of hole states of disk type ('indium flushed') InAs/GaAs and InAs/InP quantum dots. I show how strain and valence band offset affect quantum dot many-body properties: the excitonic fine structure, an important factor for efficient entangled photon pair generation, and the biexciton and charged exciton binding energies.

(Some figures may appear in colour only in the online journal)

1. Introduction

Fully *ab initio*, parameter free, modeling of million-atom self-assembled [1] or nanowire [2] quantum dots is still beyond the reach of current computers. For practical, atomistic calculation, semi-empirical approaches such as the empirical tight-binding (ETB) [3–16] or the empirical pseudopotential method (EPM) [17–24] are typically employed. The computation scheme usually starts with strain field calculation followed by the single-particle calculation followed then by the configuration interaction approach to obtain many-body (exciton, charged exciton, multi-exciton) spectra [12, 13].

Semi-empirical approaches use sets of fitted parameters determined to reproduce bulk properties such as effective masses, bulk deformation potentials and gaps at different points of the Brillouin zone [25]. Bulk derived parameters are later used for calculation of nanosize systems. Apart from potential ('bulk to nanosystem') transferability issues, one may question the reliability of important parameters describing the bulk electronic structure, that act as the input data for the empirical fitting procedure. For example, in the case of the InAs absolute valence band deformation potential (a_v) not even the sign of this quantity is unambiguously determined [27–33][1]. As semiconductor (self-assembled or nanowire) quantum dots typically are mixed material systems an additional empirical bulk parameter, the valence band offset between quantum dot and surrounding matrix material, has to be incorporated into the Hamiltonian. This 'natural' [33, 34] valence band offset (VBO) determines the depth of unstrained hole and electron confining potentials and combined with strain and deformation potentials constitutes the overall confining potential for the strained case, i.e. the 'strained' band offset. There is again a substantial uncertainty

[1] Please note that [26] uses sign convention for a_v different from many other works found in the literature.

of the natural VBO values, e.g., the reported InAs/GaAs VBO varies from 50 to 500 meV [26, 34]. The source of this discrepancy is not only due to the difference between experimental and theoretically reported values, but 'It is to be emphasized, however, that even within the framework of Kohn–Sham DFT, different computational schemes result in different predictions for the natural band offsets [...]' [33]. Li *et al* [34] state additionally that there have been 'long-standing anomalies between theory and experiment' and in their *ab initio* calculation 'For GaAs/InAs the predicted offset is increased from 0.06 eV in the previous calculation to 0.50 eV'.

For a given pair of materials (e.g. InAs/GaAs) the VBO has only one value; however, as discussed above, typically this value is practically unknown or given with large (>100 meV) uncertainty. For example, VBO = 0.06 eV is used in the EPM approach, VBO ≈ 0.17 eV is utilized in $\mathbf{k}\cdot\mathbf{p}$ studies [35], VBO = 0.23 eV is incorporated in the ETB model by Boykin *et al* [36], whereas VBO ≈ 500 meV is reported by the DFT calculations [34]. In this paper, as a practical resolution of this problem, I utilize an approach in which I perform calculations by an artificial variation of the VBO over a wide range of values. While the VBO has been considered as a merely technological parameter of lesser importance, the current study shows that it is quite the opposite. Both the single-particle and the many-body properties are affected by the choice of the VBO and caution should be exercised before applying different VBO values in a semi-empirical calculation. Abstracting from the experimental reality (there is only one, yet unknown VBO value, for a given pair of materials), the 'artificial' modification of the VBO is in itself a very interesting theoretical tool to study the effects of band confinement versus other effects such as strain. For example, the calculation of spectra for InAs/InP and InAs/GaAs lens type quantum dots using the same (nonetheless artificial) VBO helps us to understand the difference between the two types of nanosystem.

The ambiguity of the a_v and VBO bulk material values may thus affect [14] the accuracy of the qualitative description of confined valence band states in semiconductor nanosystems. This is further important as recent empirical pseudopotential method papers (e.g. [23] or [41] etc) still refer to older EPM parameterizations [22] utilizing the 'questioned' [34] VBO value ≈50 meV. Section 3.5 of the current paper discusses this point, showing that whereas 'natural' VBOs in ETB and EPM can differ significantly, strained band offsets in the two approaches are very similar.

Despite over a decade of intensive studies, the problem of a detailed understanding of holes in self-assembled InAs quantum dots is still an active field of research [37]. Ediger *et al* [38] observed characteristic spectral structure of hole states in InAs/GaAs lens type quantum dots leading to a non-trivial hole charging pattern of excitonic complexes. In our earlier work [11] we have noticed that InAs/GaAs quantum dot shape affects spectral properties of holes significantly. Recently, Gong *et al* [23, 24] have calculated electronic structure of InAs/InP lens type quantum dots and speculated that differences with respect to analogous InAs/GaAs systems are due to different common ions or different VBOs in both systems. In this paper, by a systematic VBO analysis, I show that it is not the VBO, but rather strain effects, that play a dominant role in determining the character of single-particle hole states in quantum dots.

A two-photon cascade from the quantum dot biexciton state can generate entangled photons [39] and has attracted great interest for applications in quantum information. However, anisotropic exchange splitting of bright excitons [40], induced by the asymmetry of the quantum dot confining potential [41], inhibits entanglement. Understanding the origins of fine structure splitting is thus of great importance for potential quantum dot applications. Recently, yet another scheme for entangled photon generation has been proposed [42–44], based on tuning the biexciton binding energy to zero. As in a typical experiment different excitonic complexes (both charged and neutral) are observed together, the prediction of the spectral line order [24] or binding energies (such as that of the biexciton) is usually far from trivial. To solve such issues, an inverse approach for quantum dot calculation has been recently proposed [45]. In this method one uses excitonic spectroscopy experimental data to determine quantum dot structural properties. However, the accuracy of such prediction must depend on the accuracy of the many-body calculations and indirectly on empirical parameters (such as the VBO) used in a calculation.

In this paper I compare properties of strained and unstrained systems, and study the role of quantum dot shape and the evolution of single-particle energies and charge probability densities as a function of the valence band offset. By a systematic VBO analysis, I show that strain and valence band offset effects play different, important roles in determining the character of single-particle states in quantum dots. Finally, I show that the choice of the VBO substantially affects many-body energies, in particular biexciton and trion binding energies and the excitonic fine structure.

2. Systems and methods

In the following I present a systematic study of lens and disk type InAs quantum dots, surrounded by either InP or GaAs matrix, as a function of the valence band offset, with strain effects included or artificially neglected. The height of the disk type quantum dot is $h = 3$ nm and the base diameter is $D = 16.8$ nm. For the sake of comparison with the EPM calculations [21–24], the height of the lens type dot is chosen as $h = 3.5$ nm and the base diameter is $D = 25$ nm. Both dots are located on a 1 nm thick wetting layer. The presence of the wetting layer is particularly important for disk type quantum dots as it lowers the overall quantum dot symmetry from D_{2d} to C_{2v} (lack of 'rotoinversion operation' [41]) and therefore both kinds (lens and disk) of quantum dot have low C_{2v} symmetry.

The calculation consists of several major steps: first atomic positions are calculated. There is a lattice mismatch between the quantum dot material (InAs) and the surrounding matrix material (GaAs or InP). To calculate strain relaxed positions I use the atomistic valence force field (VFF)

approach of Keating [46]. This method is described in more detail in [47, 48] and in our previous works [10, 12]. The size of the computational domain, including more than 50 million atoms, guarantees convergence of the strain distribution [49].

Due to the small lattice mismatch of InAs and InP, I neglect the piezoelectric effects in the present calculation, following similar arguments by Gong *et al* [23], who ignore piezoelectricity in the empirical pseudopotential work on InAs/InP quantum dots. Consistently, piezoelectric effects can also be neglected for low aspect ratio [7, 8, 35] lens and disk type InAs/GaAs quantum dots, where either the piezoelectricity is negligible [20] or the contribution due to second-order effects tends to cancel linear terms [35, 50]. In particular, for lens type InAs/GaAs [35] states that 'for smaller aspect ratios [...] first- and second-order effects compensate each other with respect to their impact on the electronic states'. Finally, the piezoelectricity is neglected for the sake of a fair comparison with other approaches where this effect is neglected (comment 41 from [21]).

In the second step of the calculation, the single-particle states are obtained by building the $sp^3d^5s^*$ tight-binding Hamiltonian [14, 25] and then diagonalizing the Hamiltonian by means of the Arnoldi algorithm with the matrix–vector multiplication parallelized using the *OpenMP* approach on a 48-core, shared memory system.

The single-particle tight-binding Hamiltonian for the system of N atoms and m orbitals per atom can be written in the language of the second quantization (in the site basis) in the following form:

$$\hat{H}_{\mathrm{TB}} = \sum_{i=1}^{\mathrm{N}}\sum_{\alpha=1}^{\mathrm{m}} E_{i\alpha} c_{i\alpha}^{\dagger} c_{i\alpha} + \sum_{i=1}^{\mathrm{N}}\sum_{\alpha=1,\beta=1}^{\mathrm{m}} \lambda_{i\alpha,\beta} c_{i\alpha}^{\dagger} c_{i\beta} + \sum_{i=1}^{\mathrm{N}}\sum_{j=1}^{4}\sum_{\alpha,\beta=1}^{\mathrm{m}} t_{i\alpha,j\beta} c_{i\alpha}^{\dagger} c_{j\beta} \tag{1}$$

where $c_{i\alpha}^{\dagger}$ ($c_{i\alpha}$) is the creation (annihilation) operator of a carrier on the orbital α localized on the site i, $E_{i\alpha}$ is the corresponding on-site (diagonal) energy, and $t_{i\alpha,j\beta}$ describes the hopping (off-site, off-diagonal) of the particle between the orbitals on (4) nearest neighboring sites. Coupling to further neighbors is neglected. Finally, $\lambda_{i\alpha,\beta}$ (on-site, off-diagonal) accounts for the spin–orbit interaction following the description given by Chadi [51].

As the quantum dot/matrix material lattice constants do not enter the TB Hamiltonian explicitly, strain in the TB method is accounted for by the modification of Hamiltonian matrix elements from the bulk (unstrained) values to the values modified due to bond length/angle modification. Therefore, if one uses InAs/(GaAs,InP) bulk Hamiltonian matrix elements, one is simply neglecting strain effects, so for the (artificially) unstrained [10] systems I use bulk TB parameters set from [25] and thus there is no strain contribution in the Hamiltonian, nor is the relaxation of atomic position accounted for. In other words the 'unstrained' system ('strain effects neglected') corresponds to the strain 'unrelaxed' system with the VFF step and the modification of TB parameters neglected. For strained systems, since strain effects change bond lengths and angles, strain relaxed positions are used to modify TB parameters (diagonal and off-diagonal matrix elements) following the description given in detail in my earlier work [14].

I have calculated the single-particle spectra for many VBO values from 50 to 500 meV with a 10 meV step. In this paper I use a multi-scale (multi-domain) approach, where a smaller computational domain is used for the single-particle calculation [49, 52]. Yet, as the number of atoms in the TB domain is larger than half a million, in order to make the entire process feasible I calculate only eigenenergies of several lowest electron and hole confined states. Then for several chosen VBO values I additionally calculate eigenstates and plot corresponding probability charge densities.

Finally, for several VBO values electron and hole Coulomb matrix elements (Coulomb and exchange integrals) are calculated according to the approach given in [12]. In a GW approach [53] one calculates the effective interaction W self-consistently. Not being able to carry out this calculation, I assume a statically screened Coulomb interaction. Hence the Coulomb matrix elements V_{ijkl} are given by

$$V_{ijkl} = \iint \phi_i^*(\vec{r}_1)\phi_j^*(\vec{r}_2) \times \frac{e^2}{\epsilon(\vec{r}_1,\vec{r}_2)|\vec{r}_1-\vec{r}_2|}\phi_k(\vec{r}_2)\phi_l(\vec{r}_l) \tag{2}$$

where $\epsilon(\vec{r}_1,\vec{r}_2)$ is the position-dependent dielectric function and ϕ are single-particle wavefunctions. By substituting single-particle wavefunctions in the form of linear combination of atomic orbitals, $\phi_i = \sum_{\vec{R},\alpha} b^i_{\vec{R}\alpha}|\vec{R}\alpha\rangle$, into equation (2) and then by utilizing a series of approximations [3, 12] (including the two-center approximation and retaining monopole–monopole contributions only), one obtains an approximate form of the Coulomb matrix elements [12]:

$$\begin{aligned} V_{ijkl} = {} & \sum_{\vec{R}_1}\sum_{\vec{R}_2\neq\vec{R}_1}\left[\sum_{\alpha_1} b^{i*}_{\vec{R}_1\alpha_1} b^{l}_{\vec{R}_1\alpha_1}\right] \times \left[\sum_{\alpha_2} b^{j*}_{\vec{R}_2\alpha_2} b^{k}_{\vec{R}_2\alpha_2}\right]\frac{e^2}{\epsilon|\vec{R}_1-\vec{R}_2|} \\ & + \sum_{\vec{R}_1}\sum_{\alpha_1\alpha_2\alpha_3\alpha_4} b^{i*}_{\vec{R}_1\alpha_1} b^{j*}_{\vec{R}_1\alpha_2} b^{k}_{\vec{R}_1\alpha_3} b^{l}_{\vec{R}_1\alpha_4} \times \left\langle \vec{R}_1\alpha_1, \vec{R}_1\alpha_2 \left| \frac{e^2}{|\vec{r}_1-\vec{r}_2|} \right| \vec{R}_1\alpha_3, \vec{R}_1\alpha_4 \right\rangle. \end{aligned} \tag{3}$$

The first term is the long-range, bulk-screened, contribution to the two-center integral built from the monopole–monopole interaction [54, 55] of two charge densities localized at different atomic sites. The second term is the on-site unscreened part, calculated by direct integration using atomic (Slater) orbitals [4, 5]. This approach is justified by the fact that the screening (Thomas–Fermi) radius (≈2–4 Å) is of the order of the bond length [4, 52], resulting in nearly bulk screening of off-site (long-range) term and limited screening of on-site (short-range) term contributions.

As noticed by Leung and Whaley [5], 'the precise magnitudes of on-site integrals may depend on the orbital

basis employed to evaluate them'. Lee *et al* [4] compared the results obtained with Slater-type orbitals and Gaussian-type orbitals and also studied the role of basis orthogonality. They concluded that the use of non-orthogonal Slater orbitals can be estimated to imply about 20% overall uncertainty in the on-site integrals and that tight-binding descriptions of electron–hole Coulomb interactions in quantum dots should be reliable for quantum dots larger than about 2 nm, thus much smaller than quantum dots studied in this paper. Reference [4] also states that the sensitivity of the basis orbitals decreases quickly as the dot size increases. On the other hand, Franceschetti and coworkers [55] have shown that not only Coulomb interaction, but also exchange interaction, is dominated by the long-range component, and the short-range component constitutes only about 20% of the total excitonic exchange interaction (exchange splitting of the lowest exciton states), whereas the monopole–monopole contributions capture up to 90% of the long-range component for typical III–V systems (table 1 from [55]). This conclusion is further supported by Luo and coworkers [56], showing that in general in direct-gap quantum dots (such as InAs) the electron–hole exchange interaction is dominated by the long-range component and the (small) short-range contribution scales as $1/R^3$ (R being the dot radius). In the current paper, consistent with the above discussions, the short-range, and thus basis dependent, contribution accounts for only about 1% of the ground electron–hole states Coulomb direct attraction, about 20% of the excitonic exchange splitting (dark–bright exciton splitting [40]) and about 10% of the excitonic fine structure ('anisotropic exchange' [40]) splitting (for both bright- and dark-exciton splitting). The upper bound for the basis uncertainty error can thus be expected not to exceed the above fractions and typically should be significantly lower.

The Hamiltonian for the interacting electrons and holes can be written in second quantization as [57]

$$\begin{aligned}\hat{H}_{\mathrm{ex}} = &\sum_i E_i^e c_i^\dagger c_i + \sum_i E_i^h h_i^\dagger h_i + \tfrac{1}{2}\sum_{ijkl} V_{ijkl}^{\mathrm{ee}} c_i^\dagger c_j^\dagger c_k c_l \\ &+ \tfrac{1}{2}\sum_{ijkl} V_{ijkl}^{\mathrm{hh}} h_i^\dagger h_j^\dagger h_k h_l - \sum_{ijkl} V_{ijkl}^{\mathrm{eh,dir}} c_i^\dagger h_j^\dagger h_k c_l \\ &+ \sum_{ijkl} V_{ijkl}^{\mathrm{eh,exchg}} c_i^\dagger h_j^\dagger c_k h_l. \end{aligned} \quad (4)$$

The many-body Hamiltonian for the exciton (X), the biexciton (XX) and positively (X^-) and negatively charged (X^+) trions is solved using the configuration interaction approach [12, 13].

The quantum dot and the surrounding matrix may share the same anion (e.g. InAs/GaAs) or cation (e.g. InAs/InP) or not have a common ion (e.g. InAs/GaP). In the empirical tight binding the treatment of quantum dot/material interface atoms is ambiguous. In the approach of Boykin *et al* [36], this is handled during the fitting procedure, where the diagonal Hamiltonian matrix elements of the common atom are kept the same in both materials. The value of the material band offset is incorporated into off-diagonal hopping matrix elements. This approach removes the necessity of modifying on-site matrix elements for interface atoms, but is complicated significantly for ternary systems such as InAs/InP/GaP, where, e.g., the bulk GaP properties are indirectly coupled to InAs bulk properties through the fitting process. Additionally, as VBOs are embedded into the tight-binding parameterization, a necessary, complicated refit would be needed for every different VBO value. In this paper I use an approach [14] in which I account for the valence band offset by shifting diagonal matrix elements of the quantum dot material. On-site matrix elements of interface atoms are calculated as a weighted sum of neighboring atom material on-site parameters. The Hamiltonian is built and then diagonalized for each VBO value: this gives a capability of freely tuning the VBO, suitable thus for the VBO dependence studies.

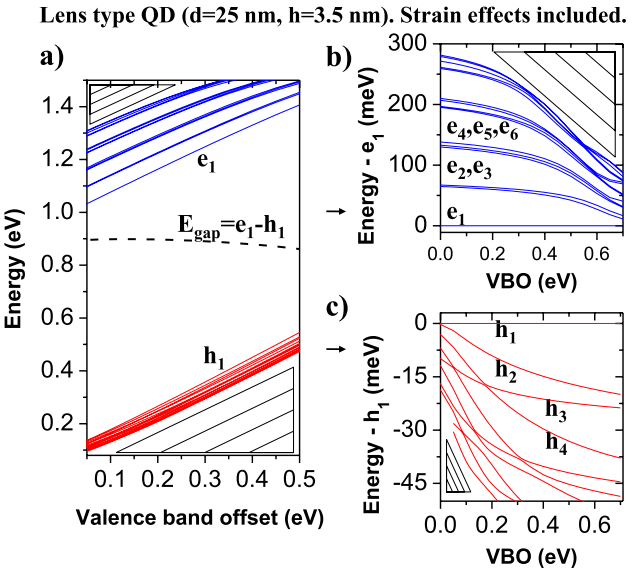

Figure 1. (a) Single-particle (electron and hole) energies and the effective gap $E_{\mathrm{gap}} = \mathrm{e}_1$–$\mathrm{h}_1$ for an InAs/GaAs lens type ($d = 25$ nm, $h = 3.5$ nm) quantum dot as a function of quantum dot (InAs) and matrix (GaAs) valence band offset (VBO), (b) single-particle electron and (c) hole energies calculated with respect to the electron (e_1) and hole (h_1) ground state energies. Patterned areas mark higher, excited states.

3. Results

Figure 1 shows the evolution of single-particle electron and hole energy levels for the lens type InAs/GaAs quantum dot as a function of the InAs/GaAs VBO. With the increasing VBO value there is an energy upshift due to overall 'reference level' (VBO) energy shift, whereas the effective band gap $E_{\mathrm{gap}} = \mathrm{e}_1$–$\mathrm{h}_1$ does not change considerably [9, 10]. In this paper I show that, whereas the above statement is generally true [9, 10, 58], the situation is far more complicated for spectral quantities other E_{gap}. To analyze the specifies of the electron and the hole spectra in the following plots I subtract the corresponding carrier ground state energy as illustrated in figures 1(b) and (c).

Valence band offset is related to ('natural' or unstrained) conduction band offset CBO through the following relation: CBO = $\mathrm{matrix}_{\mathrm{gap}}$–$\mathrm{dot}_{\mathrm{gap}}$–VBO, where $\mathrm{matrix}_{\mathrm{gap}}$ is the bulk band gap of the matrix material (GaAs or InP) and $\mathrm{dot}_{\mathrm{gap}}$

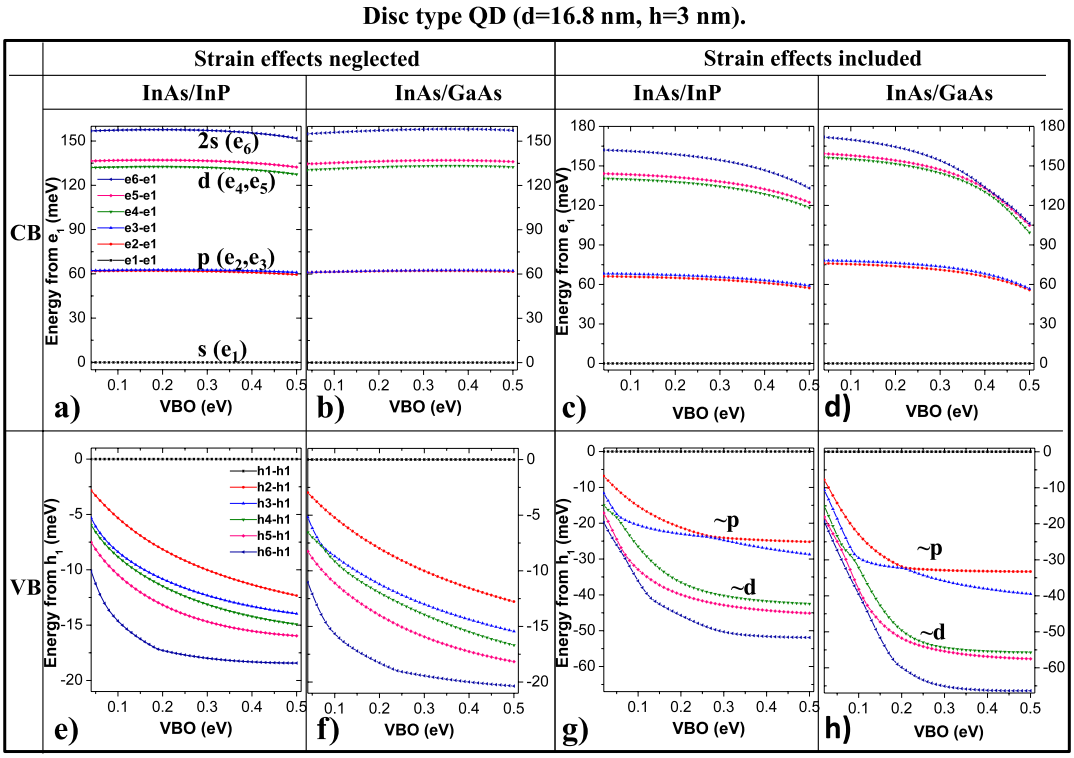

Figure 2. Electron (conduction band—CB) and hole (valence band—VB) single-particle energies calculated with respect to the electron and hole ground state energies (e_1 and h_1 correspondingly) for InAs/InP and InAs/GaAs disk type ($d = 16.8$ nm, $h = 3$ nm) quantum dots as a function of quantum dot (InAs) and matrix (GaAs or InP) valence band offset (VBO). Strain effects are either included or artificially neglected.

is the bulk band gap of the quantum dot (InAs) material. For the VBO in 50–500 meV range, the CBO varies correspondingly from ≈1 to ≈0.5 eV, with little difference between InAs/GaAs and InAs/InP cases, due to the 0.1 eV difference of InP and GaAs bulk band gaps. Increasing the VBO corresponds thus to decreasing the CBO, i.e. lower confinement of the electron states. Even though CBO is nominally larger than VBO, effects of CBO variation on electron states should be observable due to their lower confinement (effective mass).

Figures 2 and 3 show energy levels corresponding to several lowest electron (upper-CB) and hole (lower-VB) states calculated for InAs/InP and InAs/GaAs disk type and lens type quantum dots as a function of quantum dot-matrix valence band offset (VBO) with strain effects either artificially neglected or included. Figures from figures 4 to 10 show corresponding charge/probability density isosurfaces. These figures contain a substantial amount of information and will be analyzed in detail in the following part of the text.

3.1. Electron states—strain effects neglected

In an artificially unstrained InAs/(InP,GaAs) disk type quantum dot, energy spectra of lowest electron levels reveal shell-like structure (figures 2(a) and (b)), with the ground electron state of s-type character (figure 4). Despite the absence of strain and the rotational shape symmetry of the disk quantum dot, the presence of atomistic interfaces and low symmetry of the underlying crystal lattice introduces asymmetry into the Hamiltonian [20]. Thus, there are two closely spaced (splitting <1.5 meV) excited states (e_2 and e_3) of p-like character (of approximate angular momentum character $L = \pm 1$), followed by two excited (e_4 and e_5) closely spaced states (splitting ≈4 meV) of d-like character. Splittings within p and d shells are however much smaller than spacings between different shells: s–p (60 meV) and p–d (70 meV). The e_6 state (of '2s' character [20]) is separated from the lower lying d-like states e_4, e_5 by ≈20 meV, a hallmark of disk-like confinement [1]. Such structure of levels with quasi-degenerate energies corresponding to $L = 0, \pm 1, \pm 2, \ldots$ is to be expected for nominally cylindrical disk-shaped quantum dots.

Charge probability densities corresponding to several lowest electron states in an artificially unstrained InAs disk type quantum dot practically do not change in the considered range of VBO values and are very similar for both InP and GaAs matrices (figure 4). For small VBO ≈ 100 meV there is a slight elongation of the p-shell states (e_2 and e_3) along [110] and [1$\underline{1}$0] crystal axis, but otherwise these states have well defined cylindrical-like symmetry. For the VBO changing from 0.1 to 0.4 eV, the corresponding ground electron state localization inside a quantum dot drops only by 3%, i.e. from 81% to 78% in the InAs/InP case and from 86% to 83% in the InAs/GaAs case. With no strain effects included, the confinement is generally somewhat lower for InAs/InP systems when compared to InAs/GaAs due to the lower InP band gap (and thus lower CBO).

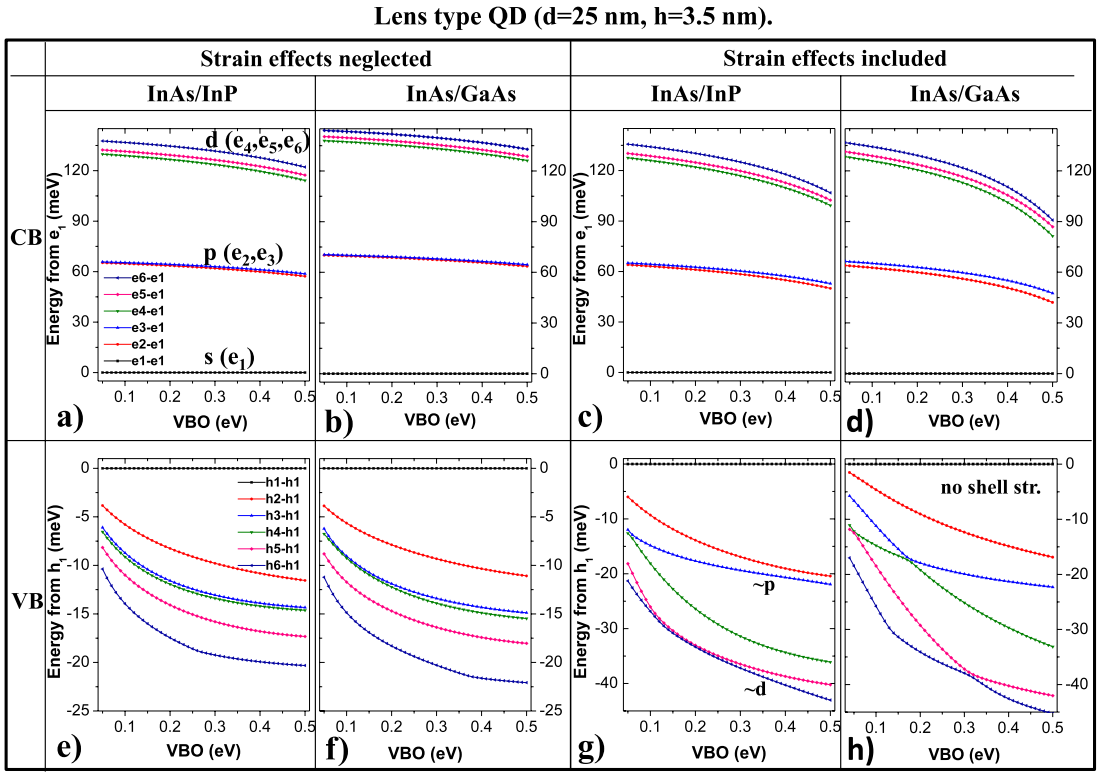

Figure 3. Electron (conduction band—CB) and hole (valence band—VB) single-particle energies calculated with respect to the electron and hole ground state energies (e_1 and h_1 correspondingly) for InAs/InP and InAs/GaAs lens type ($d = 25$ nm, $h = 3.5$ nm) quantum dots as a function of quantum dot (InAs) and matrix (GaAs or InP) valence band offset (VBO). Strain effects are either included or artificially neglected.

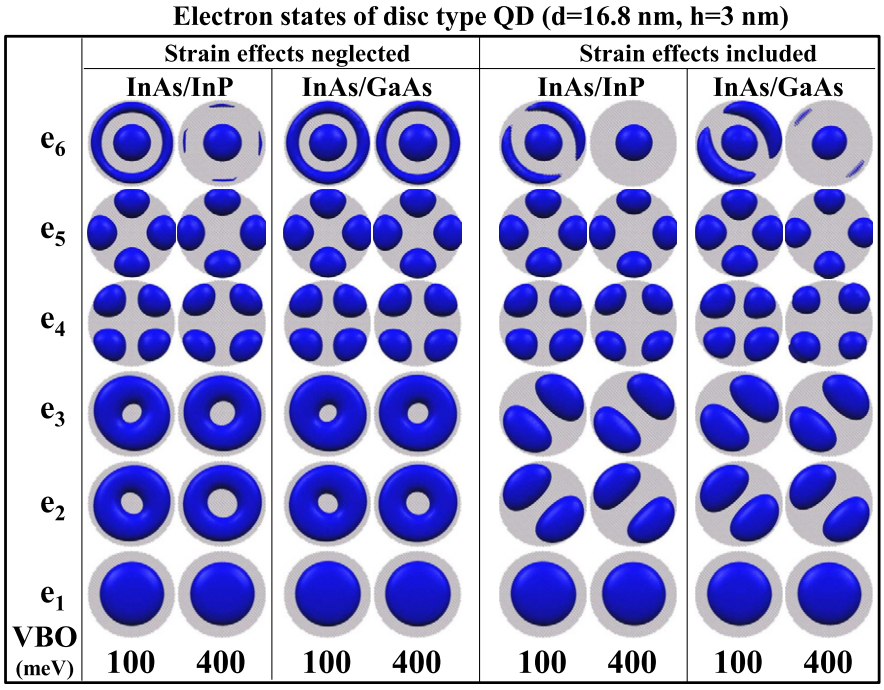

Figure 4. Electron probability density isosurfaces for InAs/InP and InAs/GaAs disk type ($d = 16.8$ nm, $h = 3$ nm) quantum dots as a function of quantum dot (InAs) and matrix (GaAs or InP) valence band offset (VBO). Strain effects are either included or artificially neglected.

For the disk type quantum dot, in the absence of strain, spacings between different shells (s–p and p–d) do not change much as a function of the VBO; however, figure 5 shows that the splitting of the electron p-shell ('p-shell anisotropy') increases monotonically (quasi-parabolically) with decreasing confinement, most likely due to the increasing role of interface

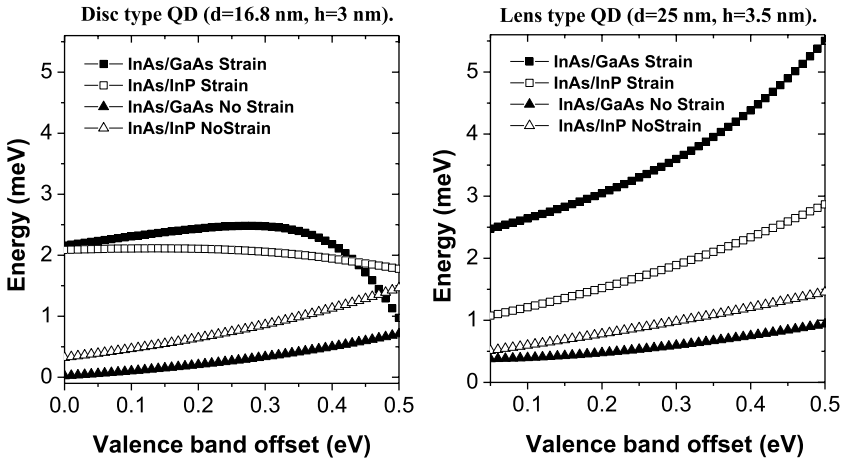

Figure 5. Splitting of the electronic p-shell calculated for InAs quantum dots of different shapes, matrix materials and as a function of quantum dot (InAs) and matrix (GaAs or InP) valence band offset (VBO).

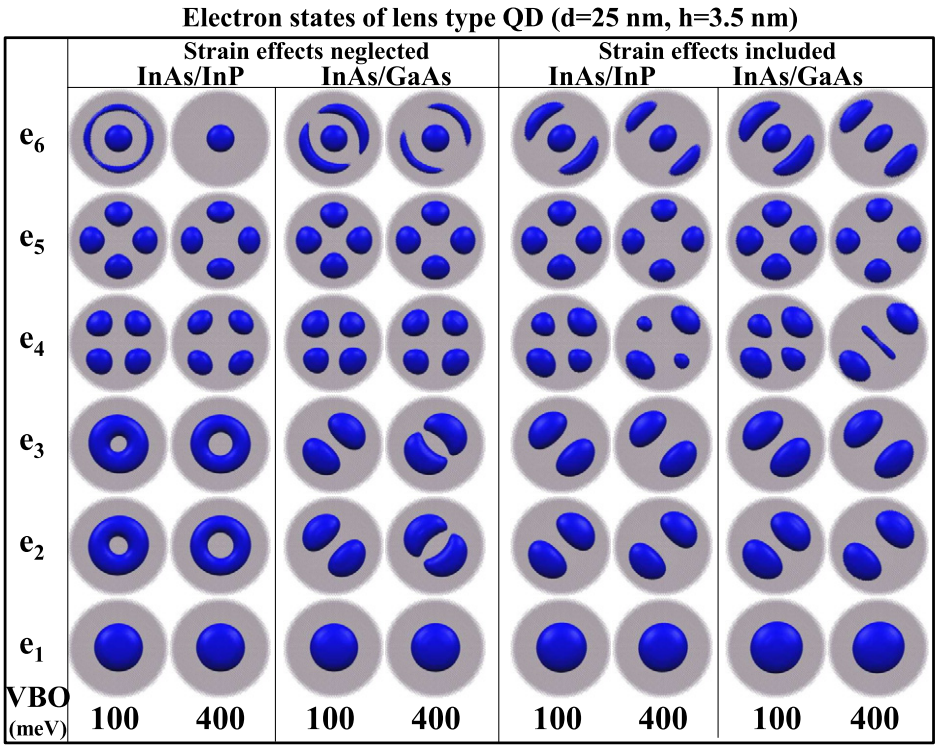

Figure 6. Electron probability density isosurfaces in InAs/InP and InAs/GaAs lens type ($d = 25$ nm, $h = 3.5$ nm) quantum dots as a function of quantum dot (InAs) and matrix (GaAs or InP) valence band offset (VBO). Strain effects are either included or artificially neglected.

effects in a progressively shallower (decreasing CBO) well for electrons. Notably, in the absence of strain, the p-shell splitting is systematically larger in the disk type InAs/InP quantum dot than in the disk type InAs/GaAs system, which I speculate can also be related to (≈5%) lower confinement of electrons in InAs/InP quantum dots. Another important difference between InAs/GaAs and InAs/InP systems is that in the first case the quantum dot and the surrounding material share a common anion (As), whereas in the latter case they share a common cation (In). Since electron wavefunctions are more localized on cation sites, having quantum dot and matrix materials with the same cations will increase the amplitude of the electron wavefunction at the interface, thus may increase the p-shell splitting for InAs/InP systems when strain effects are neglected.

In the effective mass approximation, lens type quantum dots are expected to show a 2D harmonic oscillator-like spectrum [1, 59]. In my atomistic calculations for the lens type quantum dot (figures 3(a) and (b)) I also observe the well pronounced shell structure of the electron levels and the well defined nodal structure of corresponding charge densities (figure 6). For the lens type quantum dot, electron s–p and

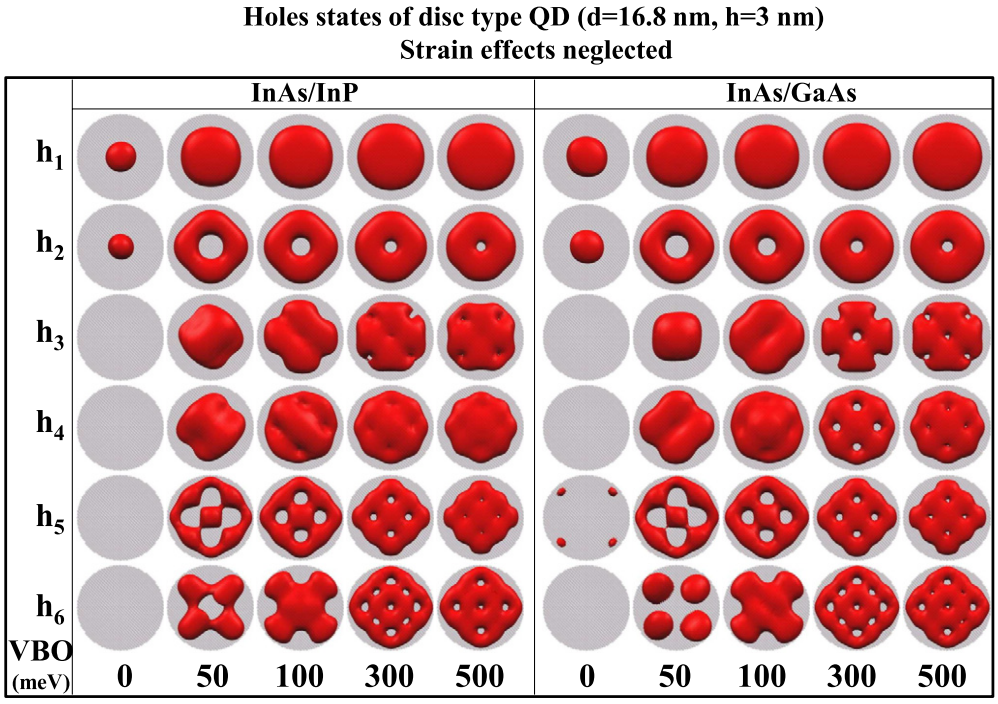

Figure 7. Hole probability density isosurfaces in InAs/InP and InAs/GaAs disk type ($d = 16.8$ nm, $h = 3$ nm) quantum dots as a function of quantum dot (InAs) and matrix (GaAs or InP) valence band offset (VBO). Strain effects are artificially neglected.

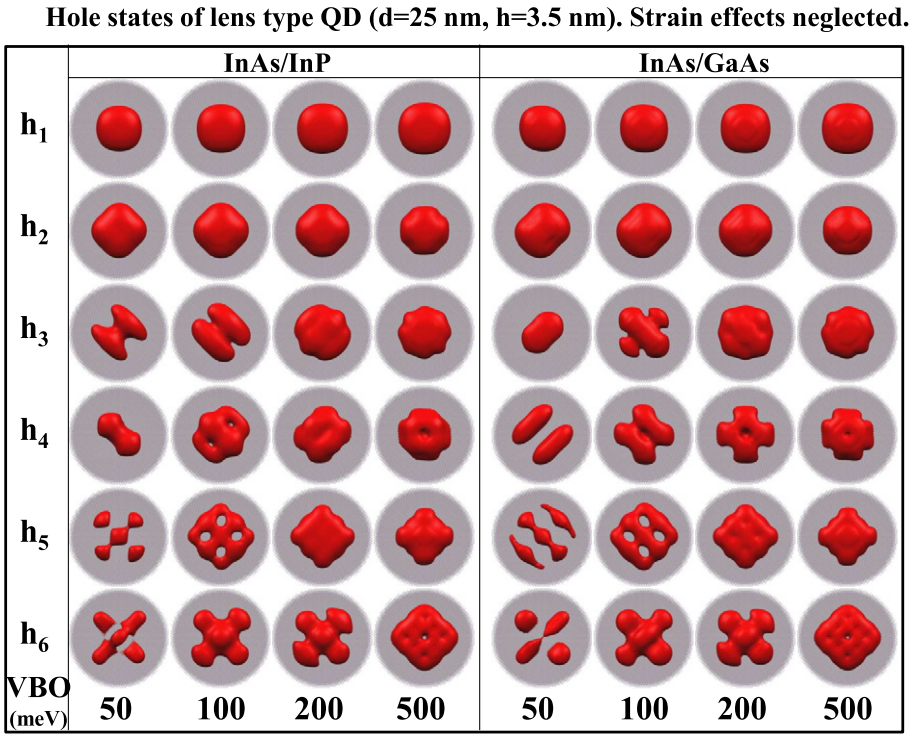

Figure 8. Hole probability density isosurfaces in InAs/InP and InAs/GaAs lens type ($d = 25$ nm, $h = 3.5$ nm) quantum dots as a function of quantum dot (InAs) and matrix (GaAs or InP) valence band offset (VBO). Strain effects are artificially neglected.

p–d level spacings slightly decrease with the increasing VBO. The ground electron state charge distribution is apparently not affected by the choice of the matrix material. The lower electron p-shell (e_2) state is localized along the [1$\underline{1}$0] crystal axis and the higher p-shell state is localized along the [110] axis in the InAs/GaAs system, whereas in the InAs/InP system both p-shell states maintain cylindrical-like symmetry. Figure 5 shows that with strain effects neglected

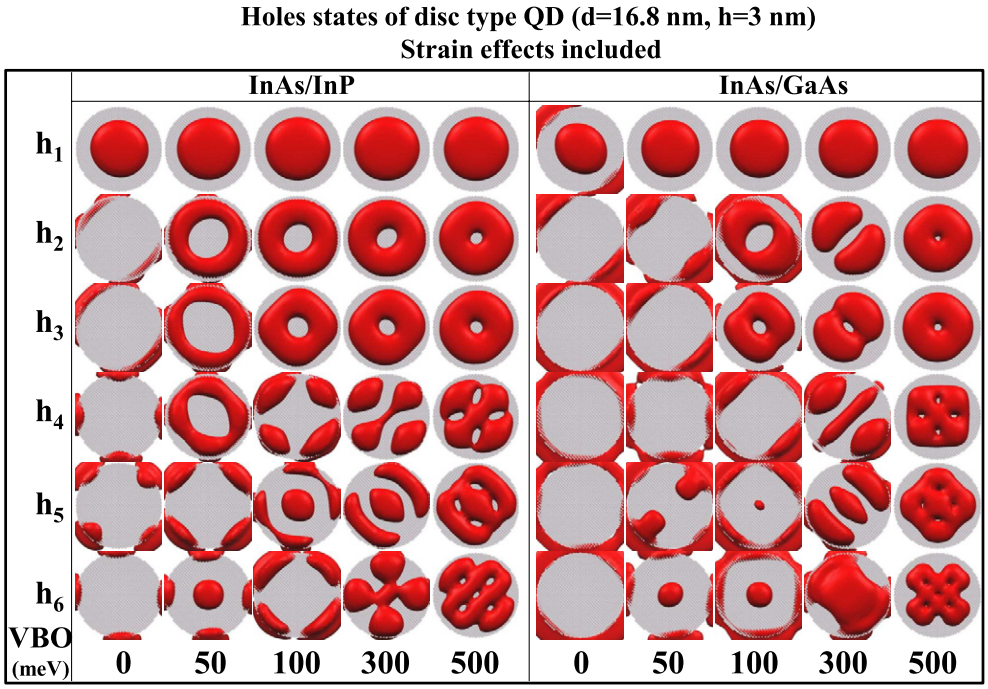

Figure 9. Hole probability density isosurfaces in InAs/InP and InAs/GaAs disk type ($d = 16.8$ nm, $h = 3$ nm) quantum dots as a function of quantum dot (InAs) and matrix (GaAs or InP) valence band offset (VBO). Strain effects are included.

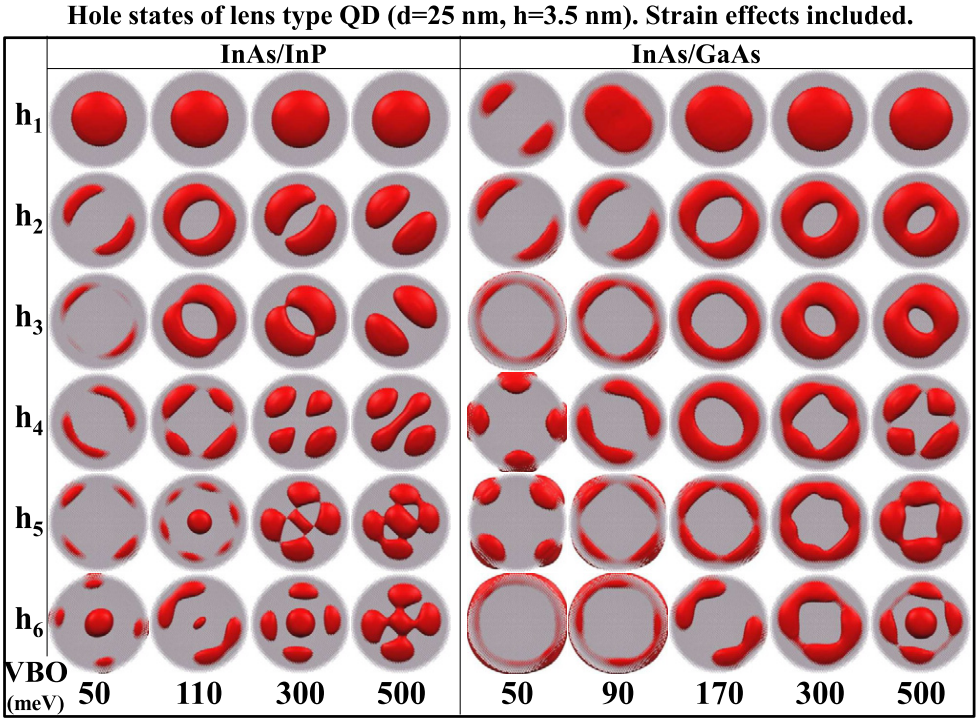

Figure 10. Hole probability density isosurfaces in InAs/InP and InAs/GaAs lens type ($d = 25$ nm, $h = 3.5$ nm) quantum dots as a function of quantum dot (InAs) and matrix (GaAs or InP) valence band offset (VBO). Strain effects are included.

the p-shell splitting depends more significantly on the absolute depth of the confining potential due to the VBO rather than on the particular quantum dot shape. Higher lying states are approximately of the same symmetry for both GaAs and InP matrices (figure 6) with similar inter-shell spacings (≈60 meV).

3.2. Electron states—strain effects included

With strain effects accounted for, the first important difference is a significant increase of the p-shell splitting for both disk and lens systems (figure 5) and the well pronounced elongation of the p-shell states along [1$\underline{1}$0] and [110] crystal

axes (figure 4). Interestingly, the p-shell state elongation for the disk type quantum dots is opposite to that of the lens type quantum dots (figure 6). Also, for the lens type quantum dot the orientation of the p-shell states is reversed [20] when compared to the strain-free case: the anisotropy due to the atomic interface is thus reversed by the anisotropy due to strain. For the highly strained InAs/GaAs disk type quantum dot, the competition of two different anisotropy sources manifests itself by a non-monotonic change of the p-shell splitting as a function of the VBO (figure 5). With strain effects included, the p-shell splitting is generally higher in lens type than in disk type quantum dots, most likely due to curved quantum dot shape or larger surface/volume ratio in lens type systems. With strain effects neglected the p-shell splitting was generally larger for InAs/InP systems; however, with strain effects included this trend reverses: the splitting is dominated by strain, and therefore is larger in InAs/GaAs than in InAs/InP systems. It is interesting to notice that, whereas electron states are built predominantly from s-type atomic orbitals (and thus should be affected predominantly by the non-directional hydrostatic strain), one expects non-zero electron–hole coupling [60], and thus one can speculate that the effects of (biaxial) strain on hole states (which will be discussed later) may also indirectly affect the electron p-shell splitting.

To summarize, the overall structure of p-shell electron states is determined by combining the matrix material, the quantum dot shape and the VBO value, and none of these factors can be neglected[2]. For confined quantum dot states (both electrons and holes), spacings between different shells (s–p, p–d, etc) increase with the increasing confining potential depth (i.e. band offset, the CBO and the VBO for electron and holes correspondingly), as expected from the quantum confinement effect (figures 2 and 3). However, splitting of levels within a given shell decreases with the increasing confinement. This is due to the progressively larger localization and effectively smaller influence of the material interface, which acts as the source of splitting. Consequently, higher-lying (d-shell) state properties are even more susceptible to the choice of the VBO due to their lower confinement.

3.3. Hole states—strain effects neglected

Interestingly, even when strain effects are neglected, the ground hole state of the considered disk and lens type quantum dots has well defined s-like symmetry (figures 7 and 8) and is predominantly of heavy-hole character. This initially may sound surprising as in this case there are no strain related heavy-hole–light-hole splitting terms in the Hamiltonian [61]. However, the quasi-two-dimensional confinement in flat quantum dot systems is efficient enough to separate the two types of hole. Alternatively, one can associate heavy-hole states with the in-plane component dominated by p_x and p_y atomic orbitals [10, 62] and affected by small, lateral confinement. Then the light-hole states are predominantly constituted by p_z orbitals and highly influenced by the vertical confinement, and thus energetically shifted away from the ground hole state.

Higher-lying states however, for both types of quantum dot, reveal complex, mixed angular momentum character (figures 7 and 8) and show no clear shell-like structure of their energy spectra (figures 2 and 3), that was so characteristic for the single-band-like confinement of the electron states. For lens type quantum dots, the first and the second excited hole states are not even of the p-like symmetry and no nodal planes are observed (figure 8).

Due to strong (>90%) confinement of hole states in the quantum dot area, with strain effects neglected, there is little difference between hole state properties with respect to the surrounding matrix (GaAs/InP). This is particularly true for large VBO values, and better confined states, where the surrounding matrix (interface effects) plays a lesser role. Consequently, there is almost one to one correspondence of charge densities for the disk type InAs/InP and InAs/GaAs quantum dot cases (figure 7).

Interestingly, even for the VBO = 0 eV and no strain effects included I still observe quantum dot hole confined states due to material properties ('effective mass') discontinuity (figure 7).

3.4. Hole states—strain effects included

Strain affects hole states significantly. For the disk type InAs/GaAs and InAs/InP quantum dots, in the 'realistic'[3] range of VBO values (210–350 meV), the structure of confined hole states is in vivid contrast to the strain-free case and resembles that of single-band electron confined states, with well pronounced shells of p-like and d-like symmetry. This effect is well visible, both in the charge distributions (figure 9) and in the energy spectra (figures 2(g) and (h)). The hole p-shell splitting lies within a few meV, i.e. much smaller than the (25–30 meV) s–p level spacing. Strain lifts heavy-hole–light-hole degeneracy [47, 61, 62] and thus effectively decouples the light-hole component of the confined hole function, leading to the single-band-like behavior of hole states in disk type ('indium flushed' [63]) quantum dots and resulting in the characteristic shell structure known also from experiment [64]. A similar conclusion may also be drawn for the disk-shaped nanowire quantum dots (which are however not placed on the wetting layer). Although we have obtained this characteristic spectrum in our earlier work [11], we have attributed it to the quantum dot shape. In this paper, I demonstrate that strain, rather than shape only, is responsible for the typical spectra of disk type quantum dots. Additionally, strain actually also leads to the characteristic harmonic oscillator-like structure of confined hole states in lens type InAs/InP quantum dots as seen in figures 3(g) and 10. In this case no shell-like structure could be observed

[2] Incorporation of piezoelectricity, necessary for high-aspect-ratio ('tall') quantum dots, would further complicate this picture.

[3] Whereas the reported InAs/GaAs VBO extreme values vary from 60 to 500 meV, the more 'realistic' or the 'recommended' [26] values can be limited to a narrower range.

with strain effects artificially neglected (figures 3(e) and 8). Therefore, strain cannot be neglected even for InAs/InP quantum dots, commonly considered 'low-strain' systems.

Hole state properties may vary significantly in the considered range of the VBO values, as VBO = 0 corresponds to no confinement other than that due to strain and material property ('effective mass') discontinuity (figure 9). For small VBO values (and lesser confinement) there is a significant leakage of the hole wavefunction into the surrounding matrix and into the highly biaxially strained wetting layer (figures 9 and 10). Strained disk type quantum dots reveal thus a strong dependence on the choice of the valence band offset; however, for VBO > 300 meV their spectral properties stabilize.

Higher-lying hole states have mixed angular momentum character and their evolution with respect to the VBO seems to depend in a complicated way on the relative evolution of different angular momentum components. In terms of state localization I can label hole states by those localized predominantly along one of two non-equivalent directions, [110] and [1$\bar{1}$0] axes correspondingly. These two species seem to evolve differently under the VBO change, leading to the observed 'level crossings' (figures 2(g) and (h)). It is important to reiterate at this point that modification of the VBO is 'artificial'; however, it constitutes a very interesting theoretical tool.

3.5. Strained valence band offset

As expected, InAs/GaAs systems are affected by strain effects more than InAs/InP due to the large lattice mismatch of the former. For a small value of VBO = 50 meV, the confining potential for holes is dominated by the strain contribution, and the character (anisotropy) of this term leads to the ground hole state of the apparent, yet unusual p-like symmetry (figure 10). I demonstrate results of the calculation for the particularly low (50 meV) VBO value, as this number is customarily utilized in the empirical pseudopotential method (EPM [21, 22]). However, I emphasize that it is the strained band offset (being the 'combination' of both VBO and a_v valence band deformation potential) that 'enters' the calculation as the actual hole confining potential [14]. Whereas the 'natural' (strain free) VBO and a_v differ significantly between the two methods (ETB, $a_v = 1$ eV; EPM, $a_v = -1$ eV), the strained band offset obtained by using the two sets of a_v and VBO parameters is very similar ≈330 meV [24]. This important conclusion is illustrated in figure 11, showing the confining potential profiles calculated for the InAs/GaAs lens type dot using the Bir–Pikus model [47]. This plot was obtained utilizing two sets of parameters: the 'recommended' ones from the review paper by Vurgaftman *et al* [26] ($a_v = +1.0$ eV, VBO = 0.21 eV) and those reported [21] by the EPM method ($a_v = -1.0$ eV, VBO = 0.05 eV). As a result, the effective confining potentials in the ETB and the EPM approaches are quite similar despite noticeably different bulk ('intermediate') target values. A more quantitative comparison of the quantum dot results obtained by the ETB and EPM was presented in our recent work [14].

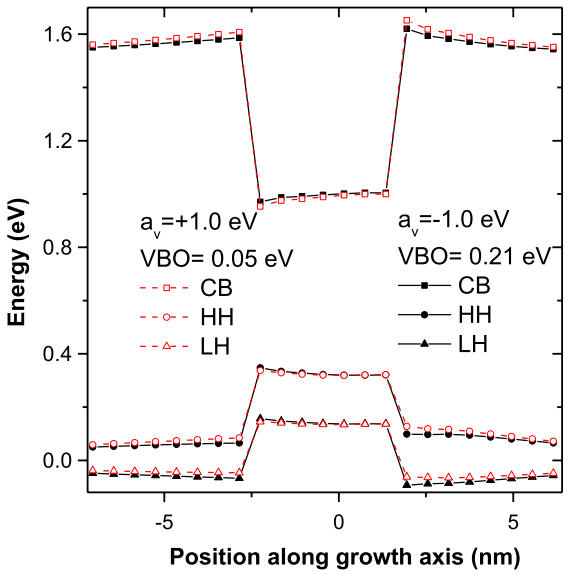

Figure 11. Strain-induced confining potentials for a InAs/GaAs lens type ($d = 25$ nm, $h = 3.5$ nm) quantum dot along the [001] axis, calculated using the Bir–Pikus model and two distinct sets of bulk VBO and a_v parameters. Conduction band (CB)—squares, heavy-hole band (HH)—circles, light-hole band (LH)—triangles.

The main difference between the lens type and disk type quantum dots comes from the fact that the disk type quantum dots are subject to 'smooth', slowly spatially varying strain (figure 12), which also induces uniform heavy-hole–light-hole splitting leading to a single-particle-like picture of hole states. In contrast, lens type quantum dots are affected by a spatially fluctuating strain due to the curved shape of quantum dots and the presence of a jagged, step-like material interface (figure 12). Electron states are built predominantly from s-type atomic orbitals and are affected only (in the Bir–Pikus formalism [47, 61, 62]) by the hydrostatic strain ($\mathrm{Tr}(\epsilon) = \epsilon_{xx} + \epsilon_{yy} + \epsilon_{zz}$), that leads predominantly to a simple energetic upward shift due to bond length contraction in the strained system. Thus electron states are less affected by highly spatially variable biaxial strain.

In contrast, the heavy-hole confining potential (in the Bir–Pikus formalism) along the growth [001] quantum dot axis going through the dot center, is given as [47] $E_{\mathrm{HH}} = a_v \mathrm{Tr}(\epsilon) - bB(\epsilon)$, where $B(\epsilon) = \epsilon_{zz} - (\epsilon_{xx} + \epsilon_{yy})/2$ is the biaxial component of strain, a_v the absolute valence band deformation potential and b the biaxial strain deformation potential ($b_{\mathrm{InAs}} = -1.8$ eV [26]). Thus, for hole states, the strain related potential shift is an interplay between the hydrostatic and biaxial strain: the biaxial strain ($-bB(\epsilon) > 0$) deepens the confinement for holes, whereas the hydrostatic strain makes the confining well in the dot region shallower ($a_v \mathrm{Tr}(\epsilon) < 0$).

Figure 13 shows the heavy-hole (in-plane) confining potential (obtained with bulk parameters from [26]) calculated for all quantum dots considered in this paper. For the lens type InAs/GaAs quantum dot one can notice a non-regular, 'jittered' spatial dependence that should affect the hole shell structure as discussed earlier in the paper. These oscillations

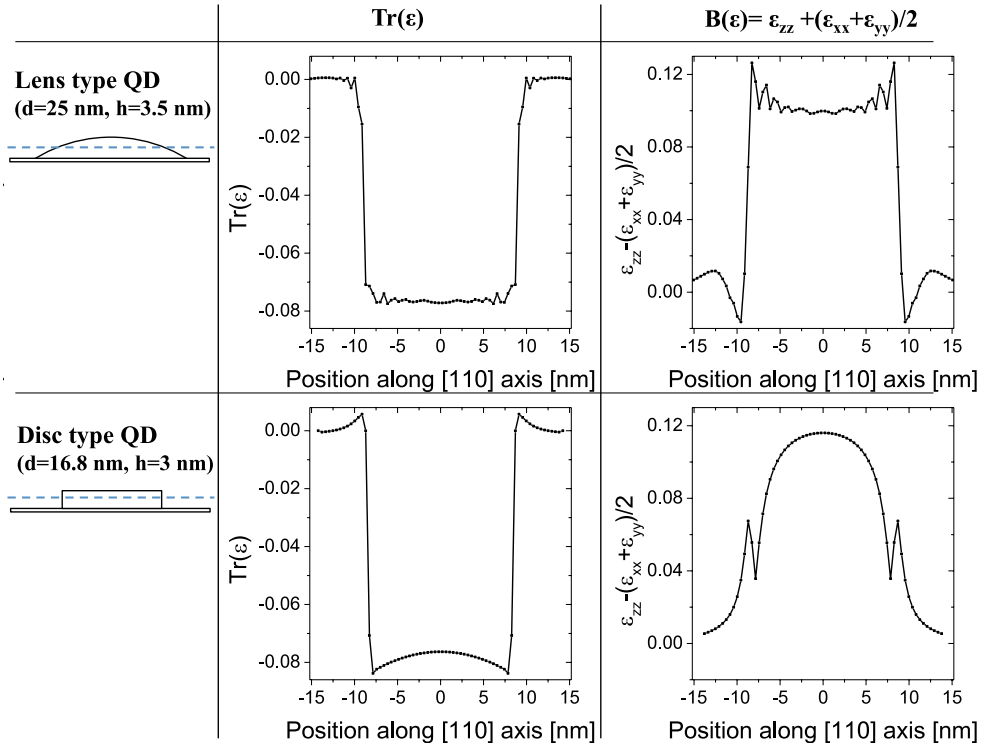

Figure 12. Trace Tr(ϵ) of the strain tensor and the biaxial $B(\epsilon) = \epsilon_{zz} - (\epsilon_{xx} + \epsilon_{yy})/2$ component of strain for a disk type ($d = 16.8$ nm, $h = 3$ nm) and a lens type ($d = 25$ nm, $h = 3.5$ nm) InAs/GaAs quantum dot. Profiles have been calculated along the [110] direction, $z = 2$ nm from the quantum dot base.

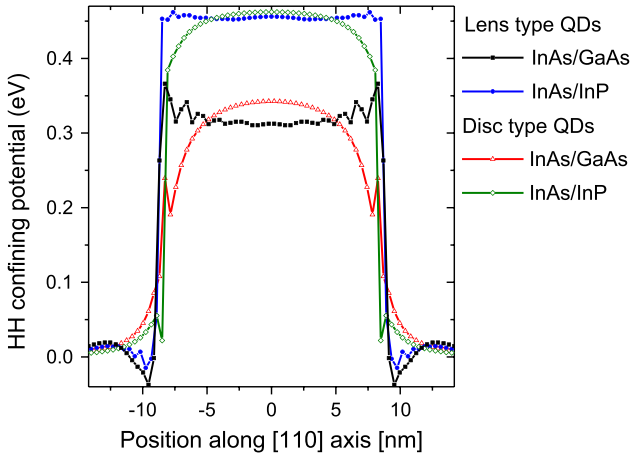

Figure 13. Strain-induced heavy-hole confining potentials for InAs/GaAs and InAs/InP disk type ($d = 16.8$ nm, $h = 3$ nm) and lens type ($d = 25$ nm, $h = 3.5$ nm) quantum dots. Profiles have been calculated using the Bir–Pikus model along the [110] direction, $z = 2$ nm from the quantum dot base.

reach up to 50 meV and even lead to formation of an attracting well for holes at the edge of the quantum dot. The situation is further complicated at the interface as the biaxial strain changes sign [47] and reverses light–heavy-hole ordering, thus affecting the valence band mixing. The interface-related oscillation seems to play a small role for the relatively 'low-strain' and high-VBO-value InAs/InP lens type quantum dot.

The complicated character of strain actually makes the InAs/GaAs lens type quantum dot hole spectra so different from those of other quantum dots. This peculiarity leads, for example, to the non-Aufbau hole charging pattern and has been confirmed by experiment [37, 38], the well established empirical pseudopotential method and also recent $k \cdot p$ calculations [35]. It is only for large [26] InAs/GaAs VBO values (>0.450 eV) that hole charge distributions of the lens type quantum dot resemble (figure 10) those of the harmonic oscillator-like states. However, even for unrealistic VBO > 0.7 eV the hole p-state splitting does not drop below 5 meV. It should be expected that this effect will be more pronounced in 'tall' (high-aspect-ratio [7]) lens, cone or pyramid type quantum dots [35].

Should accurate (order of meV) modeling of hole states be important, the choice of the 'natural' VBO will play an important role. This is again particularly noticeable for the lens type InAs/GaAs quantum dot (figure 3). In the 'recommended' range of VBO values [26] (210–350 meV), hole h_1–h_2 level spacing varies between 9 and 14 meV and spacings of higher-lying levels change even more substantially, e.g. h_3–h_4 spacing varies from 1 to 7 meV.

4. Many-body states

Strain effects and the valence band offset play a fundamental role for the single-particle states in quantum dots. Next, I calculate many-body properties of the single exciton and several excitonic complexes.

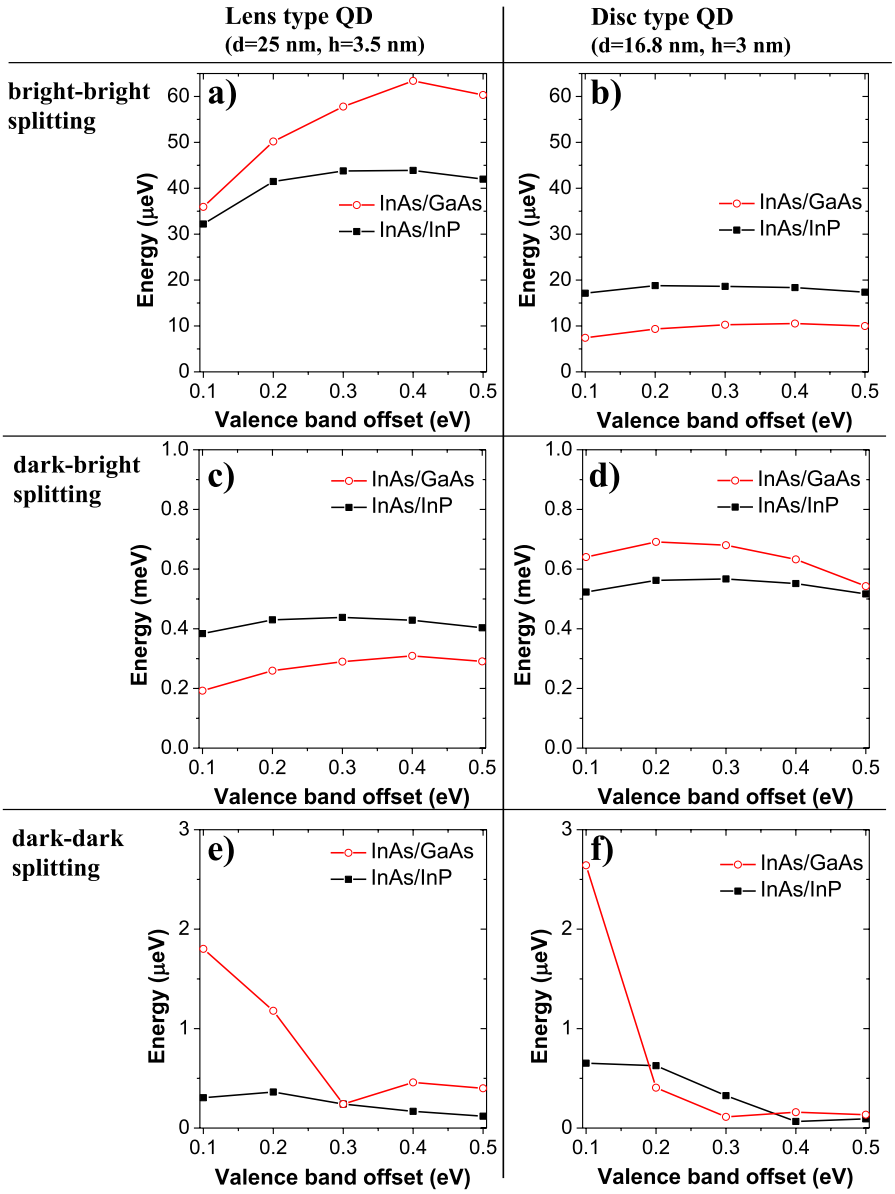

Figure 14. Excitonic fine structure for InAs/GaAs (open circles) and InAs/InP (squares) disk type ($d = 16.8$ nm, $h = 3$ nm) and lens type ($d = 25$ nm, $h = 3.5$ nm) quantum dots as a function of quantum dot (InAs) and matrix (GaAs or InP) valence band offset (VBO).

4.1. Exciton fine structure

Figure 14 shows the excitonic fine structure [40] calculated for different VBO values for the lens and disk type InAs/GaAs and InAs/InP quantum dots. The energy difference between the two bright excitonic states, the so-called bright exciton splitting (BES), is related to the confining potential anisotropy [40]. The BES is thus larger for curved shape, highly anisotropic, lens type quantum dots, reaching values varying between 40 and 60 μeV, whereas for disk type quantum dots the BES does not exceed 20 μeV. These results are in quantitative agreement with recent EPM calculations [41]; however, as noticed by the EPM researchers [65], this method systematically predicts much lower BES values than those reported in the experiment (or in the current ETB work).

For lens type quantum dots the BES varies noticeably with respect to the VBO, whereas it has almost flat VBO dependence for disk-shaped nanosystems. Although figure 14 is the result of the full many-body configuration interaction calculation [12], including single-particle states up to the d shell, the majority of the BES splitting and the overall trend is very well reproduced (not shown here) by a single electron–hole anisotropic exchange (complex) integral [4, 12, 15, 40]:

$$V_{\mathrm{eh}}^{\mathrm{b-b}} \equiv V_{\mathrm{e}_\uparrow \mathrm{h}_\Downarrow \mathrm{e}_\downarrow \mathrm{h}_\Uparrow} = \iint \frac{\mathrm{e}_\uparrow(\mathbf{r})^* \mathrm{h}_\Downarrow(\mathbf{r}')^* \mathrm{e}_\downarrow(\mathbf{r}') \mathrm{h}_\Uparrow(\mathbf{r})}{\epsilon(\mathbf{r},\mathbf{r}')|\mathbf{r}-\mathbf{r}'|}\,\mathrm{d}\mathbf{r}\,\mathrm{d}\mathbf{r}',$$

where $\epsilon(\vec{r}_1, \vec{r}_2)$ is the position-dependent dielectric function, (e) electron and (h) hole are in their ground s states and arrows correspond to carrier quasi-spins. $V_{\mathrm{eh}}^{\mathrm{b-b}}$ (as for all other Coulomb matrix elements in this paper) is calculated using equation (3).

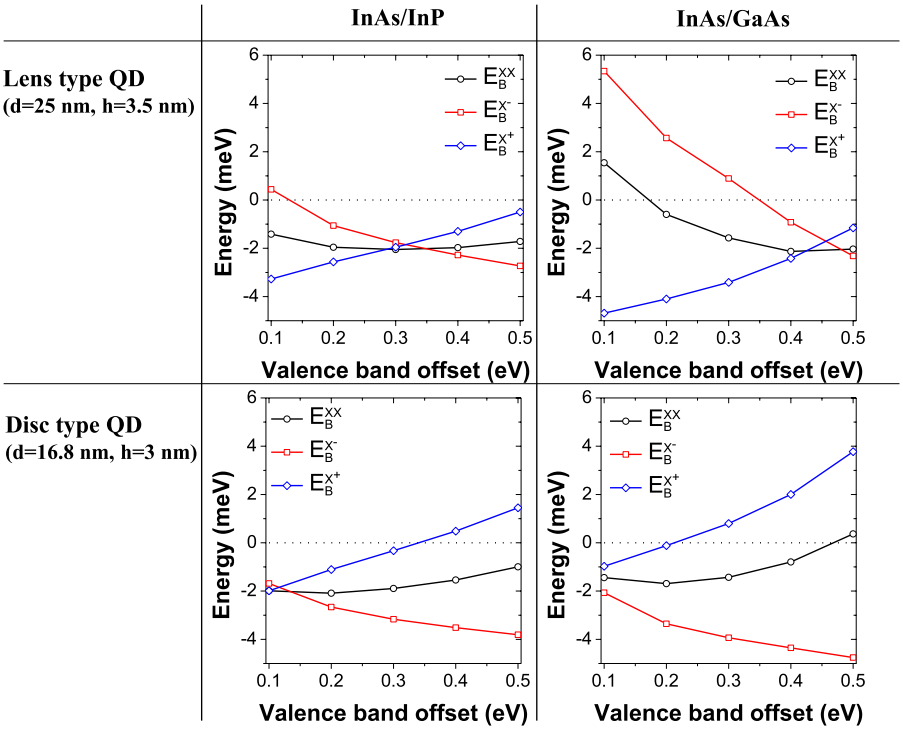

Figure 15. Biexciton XX (black circles), negatively charged X^- (red squares) and positively charged X^+ (blue diamonds) exciton binding energies, calculated with respect to the single, neutral, exciton energy, for InAs/GaAs and InAs/InP disk type ($d = 16.8$ nm, $h = 3$ nm) and lens type ($d = 25$ nm, $h = 3.5$ nm) quantum dots as a function of quantum dot (InAs) and matrix (GaAs or InP) valence band offset (VBO).

$V_{\mathrm{eh}}^{\mathrm{b-b}}$ is responsible for mixing of two bright-excitonic states ($\uparrow\Downarrow$ and $\downarrow\Uparrow$) and therefore leads to the BES. The BES is thus a two-body effect of the s-shell electron and hole spatial anisotropy and as such is not directly correlated with the electron p-shell splitting/anisotropy (figure 5).

The BES is larger for the highly strained lens type InAs/GaAs quantum dot (figure 14), as the low-symmetry (C_{2v}) of the confining potential is related to strain [20]. On the other hand the electron–hole anisotropic exchange interaction is also related to the electron–hole 'overlap' in $V_{\mathrm{eh}}^{\mathrm{b-b}}$. Therefore, similar confinement of the electron and hole may lead to larger BES. Thus, for a low-strain InAs/InP disk type quantum dot, where the electron and hole charge distributions ('envelopes') are almost identical (as seen previously in figures 4 and 9), the BES value ($\approx$18 μeV) is about twice as large as for the highly strained InAs/GaAs disk type quantum dot ($\approx$8 μeV). This is in contradiction to recent EPM calculations [66], that predict highly reduced fine-structure splitting in InAs/InP quantum dots. Finally, should the wetting layer be neglected, the BES for the disk type quantum dots would be exactly zero due to high (D_{2d}) overall (lattice and shape) quantum dot symmetry [41]. To summarize, the BES is a non-trivial function of quantum dot shape, shape and quantum dot/matrix materials.

The dark–bright exchange splitting is determined predominantly by a (real) exchange matrix element, which also conserves spin ($V_{\mathrm{eh}}^{\mathrm{d-b}} \equiv V_{\mathrm{e}_\uparrow \mathrm{h}_\Uparrow \mathrm{e}_\uparrow \mathrm{h}_\Uparrow}$). The bright–dark-exciton splitting does not vary significantly with the VBO: increased confinement of the hole seems to be assisted by the decreased confinement of the electron, and the overall electron–hole exchange integral and dark–bright-exciton splitting does not vary too much. Based on similar arguments as for the BES, the bright–dark-exciton splitting for disk type quantum dots is generally larger than in lens type quantum dots. Additionally, the bright–dark-exciton splitting is larger for cases with stronger electron–hole overlap: for the disk type quantum dot the dark–bright exchange splitting is larger in the InAs/GaAs system, while for the lens type quantum dot the dark–bright exchange splitting is larger in the InAs/InP system.

Finally, the dark-exciton splitting is a pronounced and complicated function of the VBO, especially for InAs/GaAs systems, varying over an order of magnitude for the studied VBOs. The dark-exciton splitting is generally larger for smaller VBO value; however, no clear trend regarding the matrix material is observed. It should be emphasized that, as the dark-exciton splitting values are typically of the order of a few μeV, i.e. 10^{-6} times smaller than the direct electron–hole Coulomb attraction, any practical calculation of the dark-exciton splitting, aiming for quantitative agreement with an experiment, should be supported by a careful error analysis.

4.2. XX, X^- and X^+ binding energies

Figure 15 shows the biexciton (XX) and charged trion (X^- and X^+) binding energies, measured with respect to the single-exciton energy ($E_{\mathrm{B}}^{\mathrm{XX}} = E^{\mathrm{XX}} - E^{\mathrm{X}}$, $E_{\mathrm{B}}^{\mathrm{X^-}} = E^{\mathrm{X^-}} - E^{\mathrm{X}}$, etc), for different VBO values, for lens and disk type InAs/GaAs and InAs/InP quantum dots.

For the InAs/GaAs lens type quantum dot, the biexciton binding energy varies significantly and even changes sign at VBO $\approx$ 170 meV, leading to the unbound biexciton for VBO $<$ 170 meV. Similarly, binding energies of charged excitons vary over a large range of values: there is a bound to unbound transition for X^- at VBO $\approx$ 0.35 eV. For the InAs/InP lens type quantum dot, in the 'realistic' [26–33] range of InAs/InP VBO values (300–400 meV), charged complexes even reverse their relative position in a non-trivial pattern; e.g., for VBO = 0.3 eV, one observes the following ordering of spectral lines with the increasing energy: XX, X^+, X^-, X, whereas for VBO $\approx$ 0.4 eV the order of lines is the following: X^-, XX, X^+, X.

For the InAs/GaAs disk type quantum dot ('realistic' [26–33] VBO $\approx$ 200–300 meV), the order X^-, XX, X^+ and X of spectral lines is observed, whereas for the InAs/InP disk type quantum dot (VBO $\approx$ 300–400 meV) I obtain X^-, XX, X and X^+. In all considered cases absolute binding energies and the relative order of spectral lines depend significantly on the VBO, quantum dot shape and substrate material. Therefore applying different VBO values in the excitonic calculation should be supported by a careful VBO analysis.

Excitonic binding energies must be calculated using the full many-body approach [24, 59, 67]:

$$E_{\mathrm{B}}^{\mathrm{XX}} = J_{\mathrm{ss}}^{\mathrm{ee}} + J_{\mathrm{ss}}^{\mathrm{hh}} - 2J_{\mathrm{ss}}^{\mathrm{eh}} - \Delta E_{\mathrm{corr}}^{\mathrm{XX}}$$
$$E_{\mathrm{B}}^{\mathrm{X^-}} = J_{\mathrm{ss}}^{\mathrm{ee}} - J_{\mathrm{ss}}^{\mathrm{eh}} - \Delta E_{\mathrm{corr}}^{\mathrm{X^-}}$$
$$E_{\mathrm{B}}^{\mathrm{X^+}} = J_{\mathrm{ss}}^{\mathrm{hh}} - J_{\mathrm{ss}}^{\mathrm{eh}} - \Delta E_{\mathrm{corr}}^{\mathrm{X^+}}$$

where electron–electron ($J_{\mathrm{ee}} \equiv V_{\mathrm{e_1h_1e_1h_1}}$), hole–hole ($J_{\mathrm{hh}} \equiv V_{\mathrm{h_1h_1h_1h_1}}$) and electron–hole $J_{\mathrm{eh}} \equiv V_{\mathrm{e_1h_1h_1e_1}}$ Coulomb integrals are calculated for the electron and the hole occupying their (s-shell) ground states ($\mathrm{e_1}$ and $\mathrm{h_1}$), whereas the important correction due to correlation effects ΔE_{corr} can be attributed to the configuration mixing effects with higher-lying states. In the Hartree–Fock (perturbation theory) approximation $\Delta E_{\mathrm{corr}} = 0$, whereas realistic values of binding energies ($\Delta E_{\mathrm{corr}} \neq 0$) can be calculated using the full configuration interaction method [24, 59, 67].

For example, for the lens type InAs/GaAs quantum dot, at VBO = 0.1 eV, I obtain $J_{\mathrm{ee}} = 26.28$ meV and $J_{\mathrm{eh}} = 19.54$ meV, and at the level of Hartree–Fock approximation the X^{-1} binding energy can be calculated as $\Delta E^{\mathrm{HF}}(\mathrm{X^-}) = J_{\mathrm{ss}}^{\mathrm{ee}} - J_{\mathrm{ss}}^{\mathrm{eh}} = 6.75$ meV. This value is further reduced by the correlation correction $\Delta E_{\mathrm{corr}}^{\mathrm{X^-}} = 1.41$ meV, and therefore finally $E_{\mathrm{B}}^{\mathrm{X^-}} = 5.34$ meV. On the other hand, for VBO = 0.5 meV I obtain $J_{\mathrm{ee}} = 20.88$ meV and $J_{\mathrm{eh}} = 21.68$ meV, leading to $\Delta E^{\mathrm{HF}}(\mathrm{X^-}) = -0.8$ meV. The CI calculated correlation correction is $\Delta E_{\mathrm{corr}}^{\mathrm{X^-}} = 1.52$ meV and thus we obtain $E_{\mathrm{B}}^{\mathrm{X^-}} = -2.32$ meV. Therefore, the negatively charged exciton binding energy varies from 5.34 to -2.32 meV for VBO = 0.1 eV and VBO = 0.5 eV correspondingly. The correction due to correlation mixing is important ($\approx$1.5 meV) and cannot be neglected; however, its value does change significantly as the VBO is varied. In section 4.1 I discussed that, whereas the absolute values of excitonic fine-structure splittings were results of the full configuration interaction procedure, observed trends could be analyzed in terms of a single exchange integral. A rather similar situation occurs for excitonic complex binding energies. The absolute value of the binding energy must be calculated using the many-body approach, yet its evolution with respect to the VBO can be understood at the level of Hartree–Fock (perturbation theory) approximation and several s-shell electron–hole Coulomb integrals (J_{ee}, J_{eh} and J_{hh}), whereas the correlation correction ΔE_{corr} is virtually unaffected by the choice of the VBO.

5. Summary

Valence band offset is one of the important empirical parameters for the semi-empirical tight-binding method. By a thorough VBO analysis I have shown a non-trivial interplay between the confinement potential due to the band offset and the confinement due to strain. With strain effects artificially neglected, no shell structure for holes is present, with complicated charge density distribution due to light- and heavy-hole band mixing effects. With strain effects included, heavy holes and light holes are decoupled from each other by the biaxial strain and the shell-like structure characteristic of single-band models is restored. A notable difference from this picture is observed for the strained InAs/GaAs lens type quantum dot. Due to anisotropy and inhomogeneity of the strain affected confining potential, the splittings of excited hole states dominate over shell spacings, even for the largest considered VBO value. The peculiar structure of hole levels in InAs/GaAs in lens type quantum dots, so different from InAs/InP quantum dots, originates thus from strain and is not due to the different VBO as suggested by the other studies [23]. On the other hand, the characteristic shell structure of InAs/GaAs disk type quantum dots or InAs/InP lens type quantum dots also originates from strain. In all considered cases, even for 'low-strain' InAs/InP systems, strain effects and large VBO value lead to spectral structure of hole levels known from the experiment. Therefore, strain cannot be neglected even in nominally 'low-strain' InAs/InP quantum dots, whether disk or lens shaped.

Valence band offset also affects many-body properties such as excitonic fine structure and binding energies of excitonic complexes. Exciton fine-structure splittings reported in this paper are much larger than those reported by the EPM and thus much closer to the experimentally reported values without the necessity of the inclusion of the 'ordering' effects [65]. Charged exciton and biexciton binding energies depend significantly on the depth of confinement potential (VBO) with clear distinction from the simple effective mass ('harmonic oscillator') picture. This should be emphasized, as the reliable prediction of excitonic binding energies is of key importance for so-called 'inverse approaches' [45].

The paper studies the differences between flat ('indium flushed') and lens type quantum dots and the relation between hydrostatic and biaxial strain in these systems, and quantitatively estimates the role of a jagged quantum dot/matrix material interface. The paper shows that an unrealistic p-shell symmetry of the ground hole state would be obtained if the ETB used the VBO value taken directly

from the EPM, and then discusses differences and similarities ('strained band offset') between the two approaches. Finally, the paper shows that the VBO is not merely a technological parameter, and that caution should be exercised when applying different VBO values.

Acknowledgments

This work was supported by the Foundation for Polish Science, Homing Plus Program, co-financed by the European Union within the European Regional Development Fund. The author would like to thank G W Bryant, W Jaskólski, and E Kadantsev for discussions and patient reading of the manuscript.

References

[1] Jacak L, Hawrylak P and Wojs A 1998 *Quantum Dots* (Berlin: Springer)
[2] Bjork M T *et al* 2004 *Nano Lett.* **4** 1621
[3] Schulz S, Schumacher S and Czycholl G 2006 *Phys. Rev.* B **73** 245327
[4] Lee S, Jönsson L, Wilkins J W, Bryant G W and Klimeck G 2001 *Phys. Rev.* B **63** 195318
[5] Leung K and Whaley K B 1997 *Phys. Rev.* B **56** 7455
[6] Diaz J G and Bryant G W 2006 *Phys. Rev.* B **73** 075329
[7] Usman M 2012 *Phys. Rev.* B **86** 155444
[8] Usman M 2011 *J. Appl. Phys.* **110** 094512
[9] Santoprete R, Koiller B, Capaz R B, Kratzer P, Liu Q K K and Scheffler M 2003 *Phys. Rev.* B **68** 235311
[10] Jaskólski W, Zieliński M, Bryant G W and Aizpurua J 2006 *Phys. Rev.* B **74** 195339
[11] Korkusiński M, Zieliński M and Hawrylak P 2009 *J. Appl. Phys.* **105** 122406
[12] Zieliński M, Korkusinski M and Hawrylak P 2010 *Phys. Rev.* B **81** 085301
[13] Sheng W, Cheng S-J and Hawrylak P 2005 *Phys. Rev.* B **71** 035316
[14] Zieliński M 2012 *Phys. Rev.* B **86** 115424
[15] Bryant G W, Zieliński M, Malkova N, Sims J, Jaskólski W and Aizpurua J 2010 *Phys. Rev. Lett.* **105** 067404
[16] Bryant G W, Zieliński M, Malkova N, Sims J, Jaskólski W and Aizpurua J 2011 *Phys. Rev.* B **84** 235412
[17] Wang L W and Zunger A 1999 *Phys. Rev.* B **59** 15806
[18] Wang L W, Williamson A J, Zunger A, Jiang H and Singh J 2000 *Appl. Phys. Lett.* **76** 339
[19] Canning A, Wang L W, Williamson A and Zunger A 2000 *J. Comput. Phys.* **160** 29
[20] Bester G and Zunger A 2005 *Phys. Rev.* B **71** 045318
[21] He L and Zunger A 2006 *Phys. Rev.* B **73** 115324
[22] Williamson A J, Wang L W and Zunger A 2000 *Phys. Rev.* B **62** 12963
[23] Gong M, Duan K, Li Ch-F, Magri R, Narvaez G A and He L 2008 *Phys. Rev* B **77** 045326
[24] Gong M, Zhang W, Guo G C and He L 2011 *Appl. Phys. Lett.* **99** 231106
[25] Jancu J M, Scholz R, Beltram F and Bassani F 1998 *Phys. Rev.* B **57** 6493
[26] Vurgaftman I, Meyer J R and Ram-Mohan W L R 2001 *Appl. Phys. Rev.* **89** 5815
[27] Li Y H, Gong X G and Wei S H 2006 *Phys. Rev.* B **73** 245206
[28] Wei S H and Zunger A 1999 *Phys. Rev.* B **60** 5404
[29] Van de Walle C G 1989 *Phys. Rev.* B **39** 1871
[30] Kent P R C, Hart G W L and Zunger A 2002 *Appl. Phys. Lett.* **81** 4377
[31] Kadantsev E S, Zieliński M, Korkusinski M and Hawrylak P 2010 *J. Appl. Phys.* **107** 104315
[32] Kadantsev E S, Zieliński M and Hawrylak P 2012 *Phys. Rev.* B **86** 085411
[33] Kadantsev E S and Hawrylak P 2011 *Appl. Phys. Lett.* **98** 023108
[34] Li Y-H, Walsh A, Chen A S, Yin W-J, Yang J-H, Li J, Da Silva J L F, Gong X G and Wei S-H 2009 *Appl. Phys. Lett.* **94** 212109
[35] Schliwa A, Winkelnkemper M and Bimberg D 2007 *Phys. Rev.* B **76** 205324
[36] Boykin T B, Klimeck G, Bowen R C and Oyafuso F 2002 *Phys. Rev.* B **66** 125207
[37] Blokland J H *et al* 2007 *Phys. Rev.* B **75** 233305
[38] Ediger M, Bester G, Badolato A, Petroff P M, Karrai K, Zunger A and Warburton R J 2007 *Nature Phys.* **3** 774
[39] Benson O, Santori C, Pelton M and Yamamoto Y 2000 *Phys. Rev. Lett.* **84** 2513
[40] Bayer M *et al* 2002 *Phys. Rev.* B **65** 195315
[41] Singh R and Bester G 2009 *Phys. Rev. Lett.* **103** 063601
[42] Avron J E *et al* 2008 *Phys. Rev. Lett.* **100** 120501
[43] Ding F *et al* 2010 *Phys. Rev. Lett.* **104** 067405
[44] Reimer M E *et al* 2011 *Nano Lett.* **11** 645
[45] Mlinar V, Bozkurt M, Ulloa J M, Ediger M, Bester G, Badolato A, Koenraad P M, Warburton R J and Zunger A 2009 *Phys. Rev.* B **80** 165425
[46] Keating P N 1966 *Phys. Rev.* **145** 637
Martin R M 1970 *Phys. Rev.* B **1** 4005
[47] Pryor C, Kim J, Wang L W, Williamson A J and Zunger A 1998 *J. Appl. Phys.* **83** 2548
[48] Saito T and Arakawa Y 2002 *Physica* E **15** 169
[49] Zieliński M 2012 *Acta Phys. Pol.* A **122** 312
[50] Bester G, Zunger A, Wu X and Vanderbilt D 2006 *Phys. Rev.* B **74** 081305
[51] Chadi D J 1977 *Phys. Rev.* B **16** 790
[52] Lee S, Oyafuso F, von Allmen P and Klimeck G 2004 *Phys. Rev.* B **69** 045316
[53] Onida G, Reining L and Rubio A 2002 *Rev. Mod. Phys.* **74** 601
[54] Goupalov S V and Ivchenko E L 2001 *Phys. Solid State* **43** 1867
[55] Franceschetti A, Wang L W, Fu H and Zunger A 1998 *Phys. Rev.* B **58** 13367
[56] Luo J-W, Franceschetti A and Zunger A 2009 *Nano Lett.* **9** 2648
[57] Hawrylak P and Korkusinski M 2003 *Single Quantum Dots: Fundamentals, Applications, and New Concepts* (*Topics in Applied Physics*) vol 90, ed P Michler (Berlin: Springer)
[58] Niquet Y-M and Delerue Ch 2011 *Phys. Rev.* B **84** 075478
[59] Wojs A, Hawrylak P, Fafard S and Jacak L 1996 *Phys. Rev.* B **54** 5604
[60] Kande E O 1957 *J. Phys. Chem. Solids* **1** 249
[61] Bir G L and Pikus G E 1975 *Symmetry and Strain-Induced Effects in Semiconductors* (New York: Wiley)
[62] Yu P Y and Cardona M 2005 *Fundamentals of Semiconductors: Physics and Materials Properties* (Berlin: Springer)
[63] Wasilewski Z R, Fafard S and McCaffrey J P 1999 *J. Cryst. Growth* **201/202** 1131
[64] Raymond S *et al* 2004 *Phys. Rev. Lett.* **92** 187402
[65] Singh R and Bester G 2011 *Phys. Rev.* B **84** 241402
[66] He L, Gong M, Li C-F, Guo G-C and Zunger A 2008 *Phys. Rev. Lett.* **101** 157405
[67] Zieliński M 2012 *Nanoscale Res. Lett.* **7** 265